

A Hybrid Orthosis Combining Functional Electrical Stimulation and Soft Robotics for Improved Assistance of Drop-Foot

Lucy Hodgins, Chris T. Freeman

^aSchool of Electronics and Computer Science, Faculty of Engineering and Physical Sciences, University of Southampton, Southampton, SO17 1BJ, Hampshire, United Kingdom

1 **Abstract**

2 Drop-foot is characterised by an inability to lift the foot, and affects an
3 estimated 3 million people worldwide. Current treatment methods include
4 rigid splints, electromechanical systems, and functional electrical stimulation
5 (FES). However, these all have limitations, with electromechanical systems
6 being bulky and FES leading to muscle fatigue.

7 This paper addresses the **limitations with current treatments** by develop-
8 ing a novel orthosis combining FES with a pneumatic artificial muscle (PAM).
9 It is the first system to combine FES and soft robotics for application to the
10 lower limb, as well as the first to employ a model of their interaction within
11 the control scheme. The system embeds a hybrid controller based on model
12 predictive control (MPC), which combines FES and PAM components to op-
13 timally balance gait cycle tracking, fatigue reduction and pressure demands.
14 Model parameters are found using a clinically feasible model identification
15 procedure. Experimental evaluation using the system with three healthy
16 subjects demonstrated a reduction in fatigue compared with the case of only
17 using FES, which is supported by numerical simulation results.

Keywords: Drop Foot, Soft Robotics, Electrical Stimulation, Feedback Control, Assistive Technology, Hybrid Orthosis

18 **1. Introduction**

19 Drop-foot is a condition affecting approximately 3 million people world-
20 wide [1]. It is often caused by neurological injury and is primarily associated
21 with an inability to control the tibialis anterior (TA) muscle. This leads to
22 reduced dorsiflexion, causing the foot to hang down during the swing phase
23 of the gait cycle [2]. The result is then an abnormal gait pattern, and an
24 increased risk of falls and injury [3].

25 The most common treatments for drop-foot are ankle-foot orthoses (AFOs)
26 and functional electrical stimulation (FES), with one study citing 47% of pa-
27 tients and carers having used FES and 37% having used a rigid AFO in their
28 rehabilitation [4].

29 FES involves applying electrical impulses to the peroneal nerve, leading
30 to artificial contraction of the TA muscle. Simple triggered FES systems
31 are employed commercially [5], but a variety of studies have developed more
32 advanced control methods and automated electrode configuration [6, 7, 8].
33 **FES has demonstrated improved orthotic effect when compared to AFOs**
34 **in relation to obstacle avoidance [9], as well as a long-term increase in the**
35 **volitional activity of the TA muscle [10].** However, prolonged use of FES
36 leads to muscle fatigue, resulting in physical discomfort and a reduction in
37 muscle force output [11].

38 The most basic AFOs consist of a rigid splint that either limits plantar
39 flexion or provides torque to assist dorsiflexion [9]. These have been shown to

40 improve short-term balance and walking ability [12], and there has been sig-
41 nificant research into integrating active elements such as motors, hydraulics,
42 and elastic actuators [13, 14]. These active ankle-foot orthoses (AAFOs) have
43 demonstrated success in assisting drop-foot [15] but their wide-spread use is
44 limited by their bulkiness, lack of portability, and difficulties with ensuring
45 correct joint alignment [16].

46 An alternative to the above rigid AFOs is to use soft robotics, making use
47 of compliant materials to engineer lighter, safer, and more comfortable de-
48 vices. One example is the treatment of drop-foot in children using pneumatic
49 artificial muscles (PAMs) [17], which are inexpensive, easy to make actua-
50 tors whose length can be altered by varying their internal pressure. However,
51 their performance has been limited in terms of their speed of actuation, and
52 the relatively high torque requirements mean that a large external compres-
53 sor is often required. Furthermore, depending on the method of attachment,
54 actuation can lead to strap movement, reducing the assistive torque.

55 In recent years, research has focused on treating drop-foot using a combi-
56 nation of FES and electromechanical AFOs to decrease the required stimula-
57 tion intensity and thus reduce the fatigue experienced [18, 19]. This hybrid
58 approach also reduces the AFO torque requirement, allowing for smaller,
59 more compact devices. However, current systems still have the same limita-
60 tions as purely electromechanical AFOs, the most notable being that they
61 are uncomfortable and bulky. Whilst devices have been created that combine
62 soft robotics and FES for hand rehabilitation, so far none have been designed
63 for the treatment of drop-foot, or for lower limb rehabilitation more generally.
64 A further challenge is how to control hybrid AFOs. Few hybrid control ap-

65 proaches have been applied to drop-foot, and previous approaches typically
66 involved switching between control using FES and an AAFO [18], which does
67 not fully utilise the benefits of the hybrid system (i.e. maintaining gait while
68 ensuring hybrid components minimise FES-induced fatigue and AAFO size).

69 Another hybrid approach applied electromechanical support and FES to
70 different joints [20]. This also failed to capitalise on the potential benefits of
71 a hybrid system, and was more applicable to treating multiple gait abnormal-
72 ities rather than purely drop-foot. **Model-predictive control was applied to a**
73 **hybrid system where it enabled patients with spinal cord injury to maintain**
74 **a desired knee angle [21].** However it has not yet been used in the treatment
75 of drop-foot.

76 This paper provides the following novel contributions. It develops the
77 first hybrid ankle-foot orthosis to combine FES with soft robotics. A PAM
78 is selected to reduce FES-induced muscle fatigue whilst improving comfort
79 compared to more traditional AAFOs. The paper then develops an integrated
80 FES and PAM dynamic model, together with a comprehensive identification
81 scheme suitable for clinical deployment. An optimal control approach is
82 also developed to allow FES and the PAM to be actuated simultaneously,
83 in contrast to previous approaches used to treat drop-foot. This enables
84 tracking performance and fatigue reduction to be balanced for the first time.
85 A prototype system is then created and tested on three healthy individuals
86 to evaluate the model and examine the control performance with respect to
87 both gait cycle tracking and fatigue reduction.

88 **2. Device design**

89 Figure 1 shows the proposed hybrid device. The ankle is actuated by the
 90 combined torque generated by FES stimulation (due to surface electrodes
 91 placed over the TA muscle and peroneal nerve) and PAM contraction. The
 92 PAM is anchored at one end to the lower leg, with the other end attaching to
 93 the foot. Fabric straps ensure increased user comfort compared to the rigid
 systems used in [18] and [19].

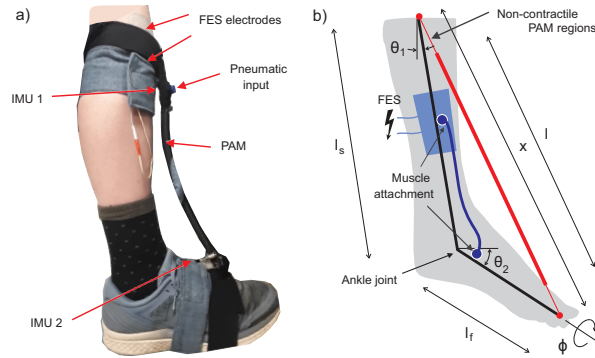


Figure 1: a) Attachment of the FES electrodes, IMUs, and PAM to the lower leg and foot, with b) corresponding sagittal plane geometry where ankle dorsiflexion is $\theta = \theta_1 + \theta_2$ and eversion/inversion is ϕ .

94

95 The PAM is manufactured from latex rubber tubing covered in a polyester
 96 braided sheath. Pressure is controlled using two solenoid valves (Adafruit
 97 industries, 1/2", 12V) driven by a compressor (Clarke tools, UK) which
 98 provides a maximum pressure of 800kPa. Inertial measurement units (IMUs)
 99 (MPU6050) attached to the knee and foot transmit data to a microcontroller
 100 (Arduino Uno SMD). These embed Kalman filters and provide angles θ , ϕ
 101 (accuracy $\pm 1.8^\circ$). FES stimulation is applied using a biphasic stimulator
 102 (Odstock Medical Ltd, UK) and controlled using pulse-width modulation

103 (PWM), with the pulsewidth varied between 0-300 μ s at a frequency of 40Hz.
 104 These components are shown in Figure 2 and will be subsequently discussed.

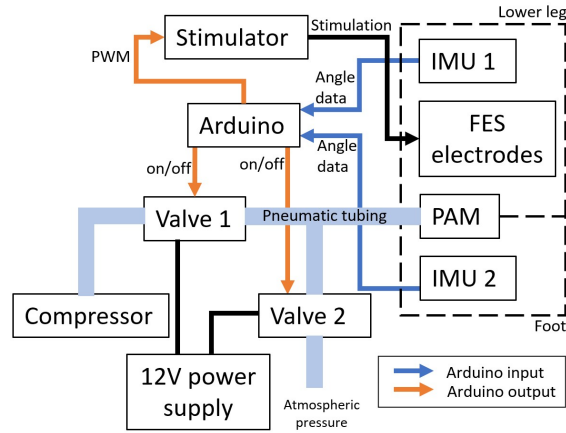


Figure 2: Schematic showing hardware components.

105

106 2.1. Modelling

107 The parameter selection and control strategy are based on a dynamic
 108 model of the hybrid system, which will be constructed by selecting and com-
 109 bining models of the individual components, as described next.

110 2.1.1. Muscle model

111 Human muscle has been modelled in a variety of different ways [22, 23, 24,
 112 25, 26], but the most common form is a Hammerstein structure comprising a
 113 static non-linear isometric recruitment curve (IRC) in series with the muscle's
 114 linear activation dynamics (LAD). The IRC relates the input stimulation
 115 signal $u(t)$ to the muscle activation, and is denoted $h_{IRC}(u)$. The LAD relates
 116 the muscle activation to muscle output force, and is denoted by transfer

117 function $G(s)$. The output is then multiplied by force-length and force-
 118 velocity relationships $f_{FL}(\theta)$ and $f_{FV}(\dot{\theta})$ to produce the overall force. Passive
 119 muscle properties will be added in Section 2.1.3.

120 There are a variety of models representing FES-induced muscle fatigue
 121 [27, 28, 29], but one of the simplest was proposed by [30] and involves mul-
 122 tiplying the output w of the IRC by a time-varying term, $f_{it}(t)$ that satisfies

$$\frac{df_{it}(t)}{dt} = \frac{(f_{min} - f_{it}(t))\lambda w(t)}{\tau_{fat}} - \frac{(1 - f_{it}(t))(1 - \lambda w(t))}{\tau_{rec}} \quad (1)$$

123 where f_{min} is the minimum fitness, λ is a scaling factor dependant on stimu-
 124 lation frequency, and τ_{fat} and τ_{rec} are the time constants for muscle fatigue
 125 and recovery respectively. The resulting overall muscle dynamics are shown
 in Figure 3.

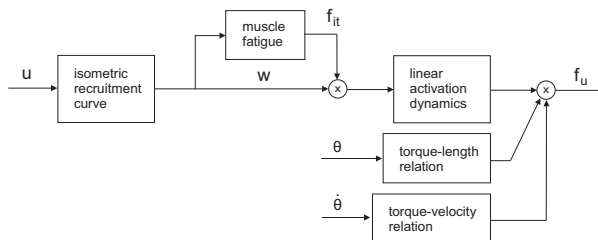


Figure 3: Block diagram showing force f_u generated by electrically stimulated TA muscle.

126

127 2.1.2. PAM and valve modelling

128 The static force produced by a PAM is commonly given by

$$f_{static}(\epsilon, p) = \pi r_0^2 p \left(\frac{3(1 - k\epsilon)^2}{\tan^2(\alpha_0)} - \frac{1}{\sin^2(\alpha_0)} \right) \quad (2)$$

129 where p is the pressure, r_0 is the initial PAM radius, α_0 is the initial braid
 130 angle, and ϵ is the strain, equal to the ratio of PAM extension to its initial

131 length. From the geometry in Figure 1, the latter is equal to

$$\epsilon = \frac{\sqrt{l_s^2 + l_f^2 - 2l_f l_s \sin(\theta_0)} - \sqrt{l_s^2 + l_f^2 - 2l_f l_s \sin(\theta)}}{l_0} \quad (3)$$

132 where θ_0 is the ankle angle when the PAM is relaxed, with l_0 later denoting
 133 the corresponding PAM length. The experimentally-derived parameter k
 134 accounts for the non-cylindrical nature of the device [31]. Relation (2) will
 135 be used in Section 4 to optimise PAM parameters, ensuring suitable force
 136 and pressure properties over the required contraction range.

137 There are a variety of dynamic models of PAM behaviour [32, 33], and a
 138 common form is obtained by adapting the above static model to include the
 139 effects of friction and surface contact forces [31] to give

$$f_p = f_{static} - f_{fric}(1/n)S_{contact}p \operatorname{sgn}(\dot{z}) \quad (4)$$

140 where $z = \epsilon l_0$ is the PAM displacement, $1/n$ is the proportion of the muscle
 141 surface rubbing against itself, $S_{contact}$ is the thread contact surface area given
 142 by

$$S_{contact} = 2\pi r_0 l_0 \frac{\sin(\alpha_0)}{(1 - k\epsilon)\sqrt{1 - \cos^2(\alpha_0)}(1 - k\epsilon)^2} \quad (5)$$

143 and f_{fric} is the dynamic friction coefficient given by

$$f_{fric} = f_k + (f_s - f_k) \exp(\dot{z}/\dot{z}_s) \quad (6)$$

144 where f_s and f_k are the static and kinetic friction coefficients respectively,
 145 and \dot{z}_s is a velocity constant.

146 While it is possible to control PAM pressure using servo valves, as done
 147 in [34], a commonly applied approach uses PWM control of on/off solenoid

148 valves [35, 36]. This reduces cost and control complexity. In both cases,
 149 PAM pressure is related to the mass flow \dot{m} through the valve by

$$\dot{p} = \frac{kRT}{v_p(z)} \dot{m}(u_v, p) - pk \frac{\dot{v}_p(z)}{v_p(z)} \quad (7)$$

150 where again $z = \epsilon l_0$, k , R , T , v_p are the specific heat ratio, gas constant,
 151 temperature, and PAM volume respectively, and u_v is the duty cycle of the
 152 valve. It is shown in [35] that a static linear relationship can accurately
 153 capture $v_p(z)$.

154 For the fastest PAM response, each valve shown in Figure 2 must be ener-
 155 gised while the other is de-energised. Defining u_{v1} and u_{v2} as the duty cycles
 156 of valves 1 and 2 respectively, the combined state is $u_v = (u_{v1}, u_{v2})$. While
 157 it is then possible to model $\dot{m}(u_v, p)$ using standard flow-rate equations, in
 158 cases where the duty cycle is high (i.e. rapid switching) this relationship is
 159 typically determined experimentally. A quadratic form validated in [37] is

$$\begin{aligned} \dot{m}(u_v, p) = & \sqrt{(p_c - p)}(m_1 u_{v1} + m_2 u_{v1}^2) \\ & - (p_a - p)(m_3 u_{v2} + m_4 u_{v2}^2) \end{aligned} \quad (8)$$

160 where p_a and p_c are atmospheric pressure and the pressure of the com-
 161 pressor respectively, and m_1 – m_4 are experimentally-derived coefficients. A
 162 bi-polynomial form was proposed in [38] but contains more parameters.

163 The overall muscle and valve dynamics are shown in Figure 4.

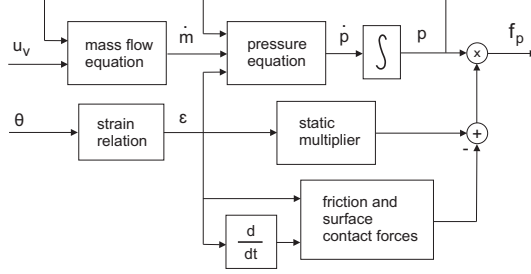


Figure 4: Block diagram showing force f_p generated by PAM valve state u_v .

164 *2.1.3. Rigid body dynamics*

165 The FES and the PAM torques actuate the ankle joint, which can be
 166 modelled by the general relationship

$$M_u(q)f_u + M_p(q)f_p = B(q)\ddot{q} + C(q, \dot{q})\dot{q} + F_s \operatorname{sgn}(\dot{q}) + F_d(q, \dot{q}) + g(q) + g_{FL}(q) + g_{FV}(\dot{q}) - J(q)h \quad (9)$$

167 where joint vector $q = [\theta, \phi]^T$, h is a vector of externally applied forces and
 168 torques, and $J(q)$ is the system Jacobian. Matrices $B(q)$ and $C(q, \dot{q})$ are
 169 the inertial and Coriolis matrices respectively, $F_d(q, \dot{q})$ is dynamic friction,
 170 $F_s \operatorname{sgn}(q)$ is the static friction, $g(q)$ comprises gravity and contact forces, and
 171 $g_{FL}(q)$ and $g_{FV}(\dot{q})$ represent the muscle elasticity and viscosity respectively.
 172 Vectors $M_u(q)$ and $M_p(q)$ are the moment arms of the TA muscle and PAM
 173 respectively. Functional forms appear in, e.g. [39, 40].

174 The component of $M_p(q)$ about the θ axis is

$$l_s \sin \left(\arccos \left(\frac{l_s^2 + x(\theta)^2 - l_f^2}{2l_s x(\theta)} \right) \right) = \sqrt{l_s^2 - \left(\frac{l_s^2 + x(\theta)^2 - l_f^2}{2x(\theta)} \right)^2} \quad (10)$$

175 where

$$x(\theta) = \sqrt{l_s^2 + l_f^2 + 2l_s l_f \sin \theta}. \quad (11)$$

176 The muscle moment arm, $M_u(q)$, is typically assumed constant [25]. It is
 177 widely assumed in the literature that the PAM acts only in a single plane
 178 and that FES pads are positioned to minimise eversion/inversion. In this
 179 case $q = \theta$ may be assumed.

180 3. Identification and Control

181 The hybrid system combines components (2)-(11) and is shown in Figure
 182 5 where

$$g(q, \dot{q}) = J(q)h - C(q, \dot{q})\dot{q} - F_s \operatorname{sgn}(\dot{q}) - F_d(q, \dot{q}) - g(q) - g_{FL}(q) - g_{FV}(\dot{q}) \quad (12)$$

$$f(q) = M_p(q) \left(\pi r_0^2 \left(\frac{3(1 - k\epsilon)^2}{\tan^2(\alpha_0)} - \frac{1}{\sin^2(\alpha_0)} \right) - f_{fric}(1/n) S_{contact} \operatorname{sgn}(z) \right) \quad (13)$$

$$h(q, \dot{q}) = M_u(q) f_{FL}(\theta) f_{FV}(\dot{\theta}) \quad (14)$$

$$d(u_v, p, q) = \frac{kRT}{v_p(l_0\epsilon)} \left(\sqrt{(p_c - p)(m_1 u_{v1} + m_2 u_{v1}^2)} - (p_a - p)(m_3 u_{v2} + m_4 u_{v2}^2) \right) - pk \frac{\dot{v}_p(l_0\epsilon)}{v_p(l_0\epsilon)} \quad (15)$$

$$y(w, w_f) = \left(\frac{(f_{min} - \frac{w_f}{w})\lambda w}{\tau_{fat}} - \frac{(1 - \frac{w_f}{w})(1 - \lambda w)}{\tau_{rec}} \right) \quad (16)$$

183

184 System parameters can be identified by extending the identification pro-
 185 cedure of [40] for an FES actuated upper limb. The resulting procedure
 186 comprises the following seven experimental tests.

187 **Definition 1** (Identification Procedure). *Consider the system shown in Fig-*
 188 *ure 5 with components (3), (12)-(16). Let an external force/torque vector*

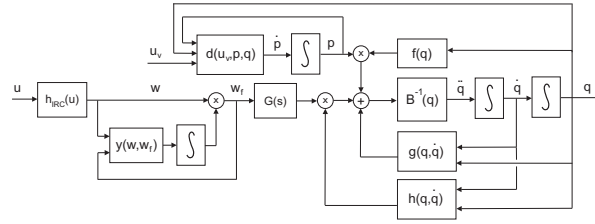


Figure 5: Complete hybrid FES/PAM ankle system dynamics.

189 h be applied to the participant's foot (e.g. by attaching a six axis sensor to
 190 the shoe and manipulating a handle attached to the sensor). Then the model
 191 components can be identified using the following procedure:

- 192 1. Apply force/torque to move the foot through a prescribed angular mo-
 193 tion, with no FES or valve input ($u = u_v = 0$). Measure h and
 194 q at sample times $\mathcal{T} = \{0, \Delta T, \dots, T\}$ and denote the data set as
 195 $\{h(t), q(t)\}_{t \in \mathcal{T}}$. Determine rigid body components $B(q)$ and $g(q, \dot{q})$ via
 196 least-squares fitting as described in [40].
- 197 2. Apply external force/torque to x foot at angle $q = 0$. Apply FES ramp
 198 signal $u(t)$ and record data $\{u(t), h(t)\}_{t \in \mathcal{T}}$. Compute FES components
 199 $h_{IRC}(u)$ and $G(s)$ via least-squares fitting, as described in [40].
- 200 3. Apply force/torque to x foot at angle $q = 0$. Apply FES signals de-
 201 scribed in [41] and record data set $\{u(t), h(t)\}_{t \in \mathcal{T}}$. Compute $\{w(t), w_f(t)\}_{t \in \mathcal{T}}$
 202 using known $h_{IRC}(u)$ and $G(s)$, and apply nonlinear minimisation to
 203 t parameters $\lambda, f_{min}, \tau_{fat}, \tau_{rec}$ such that $y(w, w_f)w = w_f$.
- 204 4. Apply force/torque to move foot through prescribed motion while also
 205 applying fixed FES level $u > 0$. Fit active FES function $h(q, \dot{q})$ to
 206 measured data set $\{h(t), q(t), u(t)\}_{t \in \mathcal{T}}$ using $f_{FL}(\theta), f_{FV}(\dot{\theta})$ parameter-
 207 isations given in [40].

- 208 5. Repeat test (4) substituting *xed* FES level by *xed* valve PAM input.
 209 Fit PAM function $f(q)$ parameters to measured data set $\{h(t), q(t), p(t)\}_{t \in [0, T]}$.
- 210 6. Attach PAM directly to a compressor and vary internal pressure p ,
 211 whilst recording $\{v_p(t), z(t)\}_{t \in [0, T]}$. Assume the linear $v_p(z(t))$ form given
 212 in [35] and t parameters via least-squares.
- 213 7. Connect valves as shown in Figure 2, without attaching device to par-
 214 ticipant, then set $u_{v2} = 0$ and record $\{\dot{m}(t), p(t)\}_{t \in [0, T]}$ for varying u_{v1} .
 215 Following this, in *ate* PAM to maximum pressure, set $u_{v1} = 0$, and
 216 record $\{\dot{m}(t), p(t)\}_{t \in [0, T]}$ for varying u_{v1} . Determine $\dot{m}(u_v(t), p(t))$ using
 217 least-squares *ting*, taking form (8). This then yields $d(u_v, p, q)$ since
 218 $v_p(z(t))$ is known and k , R , and T are constant.
- 219 Tests (6)-(7) are independent of the participant and only need to be performed
 220 *once*.

221 3.1. Control objective

222 The objective for people with drop-foot is to track the swing phase of the
 223 gait cycle, $t \in [t_{swing}, T]$ shown in Figure 6. This motivates computing the
 224 signals $u(t)$, $u_v(t)$, $t \in [0, T]$ that solve the minimisation problem

$$\arg \min J(u, u_v), \tag{17}$$

$$J(u, u_v) := \int_{t_{swing}}^T (\theta_{ref}(\tau) - \theta(\tau))^2 d\tau +$$

$$w_1 \int_0^T (1 - fit(\tau))^2 d\tau + w_2 \int_0^T p(\tau)^2 d\tau$$

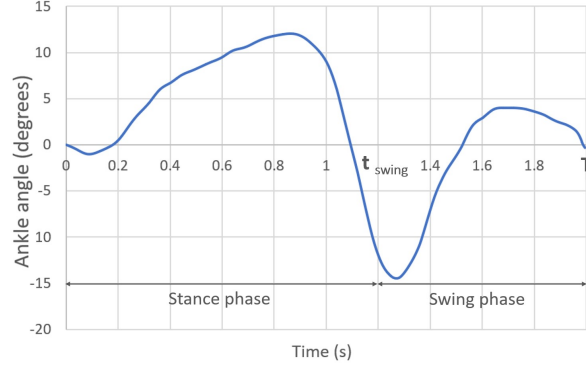


Figure 6: Changes in ankle angle over time for a typical gait cycle, based on data collected in [42].

225 subject to dynamics (3), (12)-(16) and constraints

$$\begin{aligned}
 0 < p(t) < 600, \quad t \in [0, T] \\
 0 < u(t) < 300, \quad t \in [0, T]
 \end{aligned} \tag{18}$$

226 where positive-definite weights w_1 and w_2 are used to affect a compromise
 227 between reducing FES-induced fatigue and limiting the effort required from
 228 the PAM.

229 To make the computation tractable using embedded hardware, MPC is
 230 selected due to its previous success for constrained hybrid systems. At every
 231 time instant t_k , MPC solves (17) over a receding horizon of length t_m , i.e. the
 232 time interval $t \in (t_k, t_k + t_m]$. The minimisation problem therefore becomes

$$\arg \min J(\bar{u}, \bar{u}_v), \tag{19}$$

$$\begin{aligned}
 J(\bar{u}, \bar{u}_v) := & \int_{\max\{t_k, t_{swing}\}}^{\max\{t_k+t_m, t_{swing}\}} (\theta_{ref}(\tau) - \theta(\tau))^2 d\tau + \\
 & w_1 \int_{t_k}^{t_k+t_m} (1 - fit(\tau))^2 d\tau + w_2 \int_{t_k}^{t_k+t_m} p(\tau)^2 d\tau
 \end{aligned}$$

233 where $\bar{u} = (u(t_k), u(t_k + t_m))$ and $\bar{u}_v = (u_v(t_k), u_v(t_k + t_m))$ are the inputs
 234 over the receding horizon. Minimisation (19) is solved by applying a suitable
 235 constrained nonlinear optimization algorithm to dynamics (12)-(16) and con-
 236 straints (18), starting from time $t = t_k$. Many software programs exist, e.g.
 237 SNOPT, FilterSQP, Ipopt, Knitro, Lancelot. Having computed the optimal
 238 inputs \bar{u} , \bar{u}_v , only the first element of each is then applied to the physical
 239 system. The computation is then repeated for the next time instant.

240 **Remark 2.** *The MPC solution of (19) has a feedback structure as it depends*
 241 *on the current system state, and converges to the global solution of (17) as*
 242 *the predictive horizon $t_m \rightarrow T$.*

243 3.2. Implementation

244 Solving minimisation (17) can be simplified by imposing additional struc-
 245 ture on the form of u and u_v . An obvious choice is to specify that u is the
 246 output of a PID controller that is fed by the tracking error, since this is
 247 a common choice of FES schemes and requires only three parameters (PID
 248 gains k_p , k_i , and k_d). Additionally limiting FES to only be applied for the
 249 first 0.5s of swing phase can be shown to maximise performance in experi-
 250 mental trials, since beyond this point the cost of fatigue has been found to
 251 outweigh improvements in tracking performance.

252 Signal u_v can also be simplified by specifying that the PAM is only inflated
 253 and deflated once per gait cycle. This method of control is similar to that
 254 used in [43], and requires only two parameters (contraction time t_{pr} , and
 255 relaxation time t_{pc}). These forms are then substituted into optimisation (17)

256 which simplifies to

$$\arg \min J(k_p, k_i, k_d, t_{pr}, t_{pc}), \quad (20)$$

$$J(k_p, k_i, k_d, t_{pr}, t_{pc}) := \int_{t_{swing}}^T (\theta_{ref}(\tau) - \theta(\tau))^2 d\tau + \\ w_1 \int_0^T (1 - fit(\tau))^2 d\tau + w_2 \int_0^T p(\tau)^2 d\tau$$

257 subject to the original constraints (18) and the additional constraints

$$u_v(t) = \begin{cases} (0, 1), & 0 \leq t < t_{pc} \\ (1, 0), & t_{pc} \leq t < t_{pr} \\ (0, 1), & t_{pr} \leq t < T \end{cases} \\ u(t) = \begin{cases} u, & 0 \leq t \leq (t_{swing} + 0.5) \\ 0, & t > (t_{swing} + 0.5) \end{cases} \quad (21)$$

258 Since the minimisation requires only five parameters, it is possible to perform
259 on small, low-cost hardware.

260 4. Experimental Design and Results

261 Following ethics approval (FEPS\ERGO\70971), tests were carried out
262 at the University of Southampton on three healthy adults between the ages
263 of 20-23, **in order to test the feasibility of the system.**

264 4.1. Model components

265 The PAM length l_0 and radius r_0 were calculated to satisfy $-15 < \theta < 5$
266 for $0 < p < 600$, in accordance with (2). This produced PAM dimensions of
267 9mm diameter and 30cm length.

268 *4.2. Model identification*

269 The procedure in Definition 1 was applied with the following signal and
270 functional forms chosen to minimise testing duration and resources.

271 In step (1) the rigid body dynamics components $B(q)$ and $g(q, \dot{q})$ were
272 chosen as described in [44]. In step (2) $u(t)$ was selected as a slow ramp
273 when determining $h_{IRC}(u)$, and $G(s)$ took the form given in [45, 25]. For
274 ease of measurement θ was recorded in place of h . Step (3) was replaced by
275 instead using parameter values estimated using data from [46] in order to
276 minimise muscle fatigue. Likewise in step (4) the functions $f_{FL}(\theta)$, $f_{FV}(\dot{\theta})$
277 were omitted since the angular range and velocity during a typical gait cycle
278 produces negligible effect.

279 For step (5) $h(t)$ was generated using model components previously de-
280 scribed and a measured data set $\{q(t), p(t)\}$. In step (7) the simplified valve
281 constraints (21) meant that the valve function $d(u_v, p, q)$ could be expressed
282 by $d(t_{pc}, t_{pr})$, and the valve function could then be determined experimentally
283 by measuring $p(t)$ for $u_v = (1, 0)$, $p(0) = p_a$ and $u_v = (0, 1)$, $p(0) = p_c$.

284 Table 1 gives the identification procedure fitting and prediction accuracy
285 for the complete system shown in Figure 5 with $u_v(t) = 0$. Accuracies are
286 stated as a percentage in accordance with

$$Accuracy = 100 \left(1 - \frac{\|\theta - \hat{\theta}\|_2}{\|\theta - \bar{\theta}\|_2} \right) \quad (22)$$

287 where θ is the measured ankle angle, $\hat{\theta}$ is the angle recorded by the model,
288 and $\bar{\theta}$ is the mean of θ .

289

Table 1: Fitting and prediction accuracy of full model with $u_v(t) = 0$.

Experiment no	Fitting accuracy (%)	Prediction accuracy (%)
1	48.3	44.0
2	79.3	77.9
3	56.3	46.8

290 Prediction results were obtained by splitting the data collected over a
 291 number of trials in two, with the model being fitted to one half of these
 292 before being used to predict the outcome of the other half.

293 Average fitting and prediction accuracies of 61.3% and 56.2% were ob-
 294 tained for the full model. Results were also calculated for identification of
 295 the parameters of $h_{IRC}(u)$, as given in Table 2. These were significantly
 296 higher than for the full model, with average fitting and prediction accuracies
 297 of 86.6% and 80.6% respectively.

Table 2: Fitting and prediction accuracy for the IRC curves.

Experiment no	Fitting accuracy (%)	Prediction accuracy (%)
1	85.7	83.2
2	88.9	83.9
3	85.3	74.8

298

299 *4.3. Numerical validation*

300 Optimisation weights w_1 and w_2 were selected as 5.4×10^4 and $1.35 \times$
 301 10^{-3} respectively to ensure comparable contribution of pressure and fatigue
 302 terms within the cost function. Using these weights the control cost (20) was
 303 minimised using values given in Table 3, corresponding to a cost of $J = 606$.
 304 This resulted in a tracking accuracy of 98.7%, calculated using

$$Accuracy = 100 \left(1 - \frac{\|\theta_{out} - \theta_{ref}\|_2}{\|\theta_{out} - \theta_{base}\|_2} \right) \quad (23)$$

305 where θ_{out} is the output angle of the model, θ_{ref} is the reference signal being
 306 tracked, and θ_{base} is a baseline angle used to normalise the error. This baseline
 307 was set equal to the ankle angle at the beginning of the swing phase of the
 308 gait cycle.

Table 3: Optimal simulation parameter values

	k_p	k_i	k_d	t_{pc}	t_{pr}
Hybrid	10	5	500	0.06	0.69
PAM	N/A	N/A	N/A	0.03	0.74
FES	1000	5	100	N/A	N/A

309 To investigate sensitivity, Table 4 gives the cost function for varying values
 310 of parameters k_p and k_d . The integral gain k_i was fixed at 5, and variation
 311 in this parameter resulted in little change in the cost function.

312 Table 5 gives the value of the cost function for four different values of t_{pc}
 313 and t_{pr} . The optimal tracking for the hybrid system is shown in Figure 7,
 314 along with the output angle when using purely FES and purely the PAM.

Table 4: Values of cost function (20) for FES simulation.

k_p	k_d		
	10	100	500
10	870.4	621.8	620.1
100	679.6	624.9	626.4
500	947.1	650.8	628.3
1000	1064.8	812.7	651.9

Table 5: Values of cost function (20) for PAM simulation.

$t_{pc}(s)$	$t_{pr}(s)$			
	0.2	0.4	0.6	0.8
0	2253	1095	854	963
0.2	1815	1422	1018	930
0.4	N/A	1815	1523	1637
0.6	N/A	N/A	1815	1738

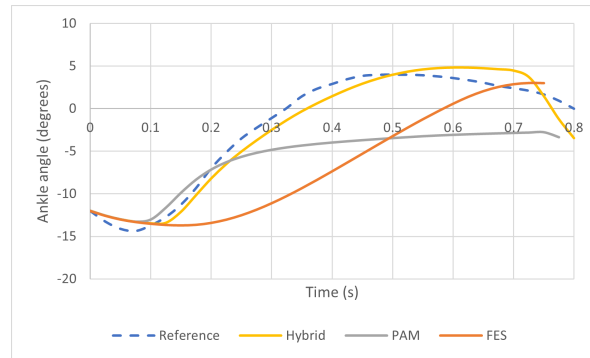


Figure 7: Tracking when using purely FES, purely the PAM, and the hybrid system with parameter values as stated in Table 3.

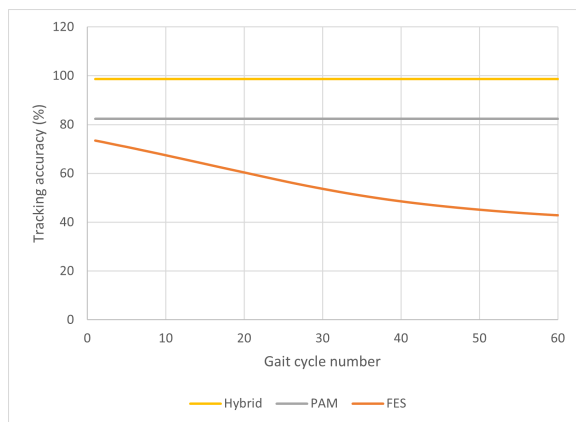


Figure 8: Comparison of tracking accuracy over subsequent gait cycles when using purely FES, purely the PAM, and with the hybrid system.

315 This reveals significantly better performance (lower cost function) when com-
 316 bining FES and the PAM than when they were applied individually.

317 Simulations were also used to investigate the long-term tracking ability
 318 of the device, as well as the difference in muscle fatigue when using the PAM
 319 compared to using purely FES.

320 Figure 8 shows the simulated tracking accuracy over the course of 60
 321 gait cycles when using purely FES, purely the PAM, and the hybrid system.
 322 The parameter values in Table 3 were again applied. This graph reveals a
 323 significant reduction in accuracy over time when using purely FES that is
 324 not seen with the hybrid approach. The initial accuracy of the FES-only and
 325 PAM-only system is also less.

326 Defining muscle fatigue as $1 - f_{it}(t)$, simulations revealed a much sharper
 327 increase in fatigue when using purely FES compared to the hybrid system, as
 328 shown in Figure 9. Furthermore the point at which muscle fatigue flattened
 329 out (i.e. where fatigue during swing phase was balanced by recovery during

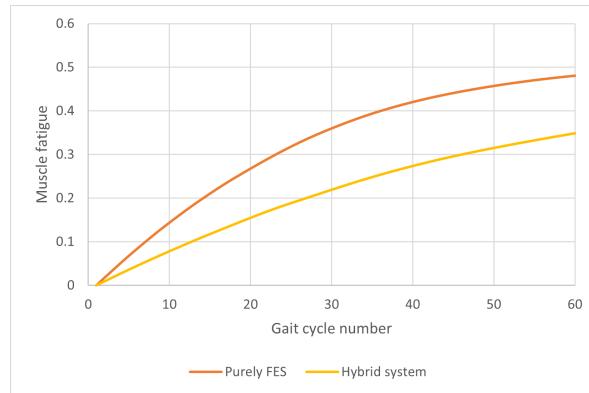


Figure 9: The progression of fatigue (defined as 1-fitness) over 60 gait cycles when using purely FES compared to the hybrid system.

stance) was greater when using FES compared to the hybrid system (0.51 compared to 0.45).

4.4. Experimental gait tracking

Following model identification each participant underwent trials to determine the tracking accuracy when using both purely FES and the hybrid system. Each ‘gait cycle’ involved applying stimulation such that the participant’s ankle tracked the swing phase shown in Figure 6, followed by a brief pause in which the foot was allowed to drop down towards the natural resting position. At the point at which the ankle reached the threshold angle indicative of the start of the swing phase (defined using data from [42]) the stimulation was applied again. This process was repeated 60 times. Each participant was allowed to rest for 20 minutes between testing the FES and hybrid systems to allow for muscle recovery.

Table 6 compares the % tracking accuracy of the FES and hybrid system averaged over 60 gait cycles for each trial. This reveals a poor tracking

345 accuracy of only 6.4% when using purely FES, compared with a much greater
 346 accuracy of 60.8% when using the hybrid system.

Table 6: Experimental gait cycle tracking accuracies.

Participant no	FES tracking accuracy (%)	Hybrid system tracking accuracy (%)
1	-22.3	49.4
2	8.47	51.8
3	33.0	81.2

347

348 Figure 10 shows representative results for the gait cycle tracking accuracy
 349 over the course of 60 gait cycles when using purely FES, alongside that when
 350 using the hybrid system. The general trend reveals a decrease in tracking
 351 ability when using FES which contrasts with the hybrid system, for which
 352 tracking accuracy remains fairly constant. This is consistent with the simu-
 353 lation results given in Figure 8.

354 4.5. Experimental fatigue results

355 In order to measure changes in muscle fatigue, a stimulation pulse of
 356 $300\mu s$ intensity and 1s duration was applied at the start and end of both gait
 357 cycle tracking experiments. The muscle response to the first pulse acted as a
 358 baseline for initial muscle fitness, which was then compared to the response
 359 to the final pulse in order to quantify fatigue.

360 Table 7 shows the changes in ankle angle, $\Delta\theta$, in response to the $300\mu s$
 361 stimulation input before and after the gait cycle tracking experiments for

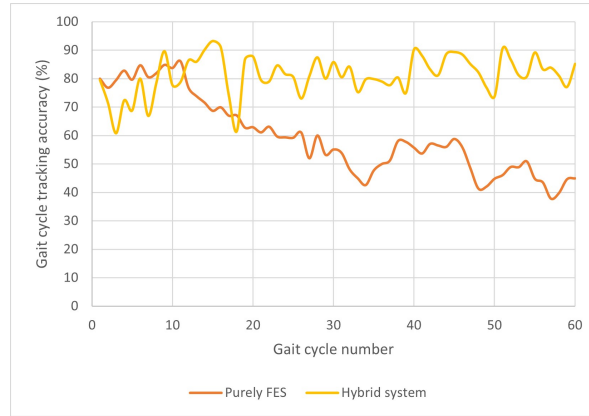


Figure 10: Comparison between the experimental tracking accuracy for participant 3 when using purely FES compared to the hybrid system.

362 both the FES and hybrid system. In all cases a significantly smaller muscle
 363 response was observed after 60 gait cycles using FES compared to before,
 364 but this same decrease was not seen when using the hybrid system.

Table 7: Change in muscle response ($^{\circ}$) due to stimulation for purely FES and hybrid control, pre and post gait tracking.

Experiment	FES		Hybrid	
	$\Delta\theta$ pre	$\Delta\theta$ post	$\Delta\theta$ pre	$\Delta\theta$ post
1	17.4	2.18	9.9	9.85
2	33.91	9.57	14.16	35.9
3	29.02	18.83	22.2	30.95

365 5. Discussion

366 The motivation behind the hybrid approach proposed in this paper was
 367 to reduce the disadvantages associated with using either purely FES or soft

368 robotics when assisting people with drop-foot. These include FES-induced
369 muscle fatigue and the reduction in performance that can occur due to poor
370 AFO fitting.

371 A primary benefit of this device is its ability to reduce fatigue when com-
372 pared to using purely FES. This has been successfully demonstrated in sim-
373 ulation, and experimental results confirm a significant benefit. Furthermore,
374 the hybrid device demonstrates a clear improvement over using purely FES
375 when considering long-term tracking accuracy, as shown in Figures 8 and 10.
376 Another advantage of the hybrid approach is the increased gait tracking ac-
377 curacy observed both in simulation and experimental results when compared
378 to using either FES or the PAM individually.

379 In terms of the usability of the system, there are still some challenges
380 that need to be overcome. Studies have revealed that the most important
381 features of an assistive device to impact on user experience are comfort and
382 ease of setup/use [4], properties that are limited in the proposed system by
383 the need for a compressor to actuate the PAM. While the current setup re-
384 quires the user to be tethered to an external compressor, a number of similar
385 soft robotic systems have succeeded in attaching a light-weight compressor
386 to the trunk of the body [47, 48]. This positioning allows for total portabil-
387 ity whilst reducing the mass of the system at the extremities, increasing user
388 comfort. It is therefore a potential solution. The total weight of the proposed
389 ankle-foot orthosis is 102g, significantly less than similar pneumatic AFOs,
390 e.g. [43, 49, 50].

391 With regards to ease of setup, successful FES stimulation currently requires
392 correct positioning of the electrodes, which may be difficult for users to

393 achieve. Furthermore, the requirement to carry out the identification pro-
394 cedure in Definition 1 significantly increases setup time. These issues are
395 addressed in the next section.

396 A secondary aim of this paper, alongside the fabrication of a physical
397 device, was to present a model that could be used to predict optimal con-
398 trol parameter values. The proposed model and identification procedure was
399 unique in its ability to combine both FES and soft robotics. It also ac-
400 counted for the occurrence of muscle fatigue, a factor which is often ignored
401 when identifying muscle dynamics in similar papers (e.g. [51]). The model of
402 FES muscle response was found to have relatively high fitting and prediction
403 accuracy when compared with similar FES identification papers (e.g. [52]).
404 The control approach was presented as a general minimisation problem, en-
405 abling the designer to choose either an MPC solution form, or to impose
406 additional constraints that simplify the computation and allow solutions to
407 be implemented on low cost, portable hardware.

408 6. Conclusions and Future Work

409 This paper is the first to demonstrate the feasibility of combining FES and
410 soft robotics for the treatment of drop-foot. A device was created combining
411 a PAM with FES, with all three experiments demonstrating a significant
412 decrease in the fatigue experienced when using the hybrid system compared
413 to purely FES. This paper has also presented a novel simulation used to
414 predict optimal parameters for hybrid control. This further revealed the
415 benefit of the system in terms of minimising muscle fatigue and maximising
416 tracking accuracy.

417 Future work focuses primarily on further improving the tracking ability
418 of the experimental system by implementing a more advanced control ap-
419 proach, before increasing the number of participants the device is tested on.
420 Additionally, the results when testing on persons with drop-foot may be dif-
421 ferent to those seen for healthy individuals, so following this the system will
422 be validated with a suitable sample of the former group. A questionnaire will
423 also capture user perceptions of the system to inform further development.

424 Furthermore, if the device were to be used for rehabilitation outside of
425 a clinical environment the size of the hardware would need to be reduced,
426 using a smaller compressor and valve setup and miniaturising the electronics.
427 An electrode array could be used to reduce the need for accurate electrode
428 positioning, and multiple model switched adaptive control (MMSAC) used to
429 reduce identification time. MMSAC works by defining a set of possible model
430 parameters that might represent the true system. It then implements a bank
431 of estimators that compute which model most accurately fits the measured
432 data, and applies the controller designed for the corresponding model. Initial
433 feasibility of combining MMSAC and electrode arrays was established in [53].

434 **7. Conflict of Interest**

435 None declared.

436 **8. Funding**

437 None received.

438 **9. Ethical Approval**

439 Experimental trials were carried out following approval from University
440 of Southampton Ethics Committee (FEPS\ERGO\70971). All participants
441 gave written informed consent.

References

- [1] C. L. Barrett, P. N. Taylor, The effects of the odstock drop foot stimulator on perceived quality of life for people with stroke and multiple sclerosis, *Neuromodulation* 13 (1) (2010) 58–64.
- [2] J. Graham, Foot drop: Explaining the causes, characteristics and treatment, *British Journal of Neuroscience Nursing* 6 (4) (2010) 168–172. doi:10.1051/mateconf/20178702031.
- [3] E. W. Peterson, C. C. Cho, M. L. Finlayson, Fear of falling and associated activity curtailment among middle aged and older adults with multiple sclerosis, *Multiple sclerosis journal* 13 (9) (2007) 1168–1175. doi:10.1177/1352458507079260.
- [4] A.-M. Hughes, J. H. Burridge, S. H. Demain, C. Ellis-Hill, C. Meagher, L. Tedesco-Triccas, R. Turk, I. Swain, Translation of evidence-based assistive technologies into stroke rehabilitation: users’ perceptions of the barriers and opportunities, *BMC Health services research* 14 (1) (2014). doi:10.1186/1472-6963-14-124.
- [5] G. York, S. Chakrabarty, A survey on foot drop and functional electrical

- stimulation, *International Journal of Intelligent Robotics and Applications* 3 (2019) 4–10. doi:<https://doi.org/10.1007/s41315-019-00088-1>.
- [6] A. Page, Repetitive control and electrode array pattern selection for FES-based drop-foot assistance, Ph.D. thesis, University of Southampton (Sept 2020).
- [7] Y.-L. Chen, S.-C. Chen, W.-L. Chen, C.-C. Hsiao, J.-S. Kuo, T.-S. and Lai, Neural network and fuzzy control in FES-assisted locomotion for the hemiplegic, *Journal of Medical Engineering & Technology* 28 (1) (2004) 32–38. doi:[10.1080/03091900310001211523](https://doi.org/10.1080/03091900310001211523).
- [8] T. Seel, C. Werner, J. Raisch, T. Schauer, Iterative learning control of a drop foot neuroprosthesis : Generating physiological foot motion in paretic gait by automatic feedback control, *Control Engineering Practice* 48 (2016) 87–97. doi:[10.1016/j.conengprac.2015.11.007](https://doi.org/10.1016/j.conengprac.2015.11.007).
- [9] R. van Swigchem, H. van Duijnhoven, J. den Boer, A. C. Geurts, V. Weerdesteyn, Effect of peroneal electrical stimulation versus an ankle-foot orthosis on obstacle avoidance ability in people with stroke-related foot drop, *Phys. Ther.* 92 (3) (2012) 398–406. doi:[10.2522/ptj.20100405](https://doi.org/10.2522/ptj.20100405).
- [10] A. Kottink, H. Hermens, A. Nene, M. Pt, C. Groothuis-Oudshoorn, M. IJzerman, Therapeutic effect of an implantable peroneal nerve stimulator in subjects with chronic stroke and footdrop: A randomized controlled trial, *Physical therapy* 88 (2008) 437–48. doi:[10.2522/ptj.20070035](https://doi.org/10.2522/ptj.20070035).

- [11] J. J. Wan, Z. Qin, P. Y. Wang, Y. Sun, X. Liu, Muscle fatigue: general understanding and treatment, *Experimental & molecular medicine* 49 (10) (2017) 384. doi:10.1038/emm.2017.194.
- [12] S. F. Tyson, R. M. Kent, Effects of an ankle-foot orthosis on balance and walking after stroke: A systematic review and pooled meta-analysis, *Archives of Physical Medicine and Rehabilitation* 94 (7) (2013) 1377–1385. doi:https://doi.org/10.1016/j.apmr.2012.12.025.
- [13] J. Kim, S. Hwang, R. Sohn, Y. Lee, Y. Kim, Development of an active ankle foot orthosis to prevent foot drop and toe drag in hemiplegic patients: A preliminary study, *Applied Bionics and Biomechanics* 8 (3-4) (2011) 377–384. doi:10.3233/ABB-2011-0008.
- [14] T. Kikuchi, S. Tanida, K. Otsuki, T. Yasuda, J. Furusho, Development of third-generation intelligently controllable ankle-foot orthosis with compact mr fluid brake, 2010 IEEE International Conference on Robotics and Automation (2010) 2209–2214doi:10.1109/ROBOT.2010.5509729.
- [15] V. Arnez-Paniagua, H. Rifañ , Y. Amirat, S. Mohammed, Adaptive control of an actuated-ankle-foot-orthosis, 2017 International Conference on Rehabilitation Robotics (ICORR) (2017) 1584–1589doi:10.1109/ICORR.2017.8009474.
- [16] A. M. Dollar, H. Herr, Lower extremity exoskeletons and active orthoses: Challenges and state-of-the-art, *IEEE Transactions on Robotics* 24 (1) (2008) 144–158. doi:10.1109/TRO.2008.915453.

- [17] N. Z. Ishak, S. Mohamaddan, A. M. N. A. Kamaruddin, H. Khamis, S. Yamamoto, S. Z. M. Dawal, Development of ankle foot orthosis (AFO) using pneumatic artificial muscle for disabled children, *MATEC Web of Conferences* 87 (2017) 016007. doi:10.1051/mateconf/20178702031.
- [18] P.-G. Jung, W. Huo, H. Moon, Y. Amirat, S. Mohammed, A novel gait phase detection algorithm for foot drop correction through optimal hybrid FES-orthosis assistance, in: *2021 IEEE International Conference on Robotics and Automation (ICRA)*, 2021, pp. 10391–10397. doi:10.1109/ICRA48506.2021.9561497.
- [19] H. R. Kobravi, Y. Farzaneh, M. Faryar Majd, M. Sheikh, A. Akbarzadeh Tootoonchi, A human interactive hybrid FES-robotic system applicable to improvement of foot drop after stroke: Case report of a patient with chronic stroke, *The Archives of Bone and Joint Surgery* 8 (6) (2020) 744–747. doi:10.22038/abjs.2020.48595.2410.
- [20] V. Krishnamoorthy, W.-L. Hsu, T. Kesar, D. Benoit, S. Banala, R. Perumal, V. Sangwan, S. Binder-Macleod, S. Agrawal, J. Scholz, Gait training after stroke: A pilot study combining a gravity-balanced orthosis, functional electrical stimulation, and visual feedback, *Journal of neurologic physical therapy : JNPT* 32 (2009) 192–202. doi:10.1097/NPT.0b013e31818e8fc2.
- [21] N. A. Kirsch, X. Bao, N. A. Alibeji, B. E. Dicianno, N. Sharma, Model-based dynamic control allocation in a hybrid neuroprosthesis, *IEEE Transactions on Neural Systems and Rehabilitation Engineering* 26 (1) (2018) 224–232. doi:10.1109/TNSRE.2017.2756023.

- [22] W. Durfee, K. Palmer, Estimation of force-activation, force-length, and force-velocity properties in isolated, electrically stimulated muscle, *IEEE Transactions on Biomedical Engineering* 41 (3) (1994) 205–216. doi:10.1109/10.284939.
- [23] M. Ferrarin, A. Pedotti, The relationship between electrical stimulus and joint torque: a dynamic model, *IEEE Transactions on Rehabilitation Engineering* 8 (3) (2000) 342–352. doi:10.1109/86.867876.
- [24] Z. Hussain, M. Tokhi, Modelling of muscle extension and flexion for FES-assisted indoor rowing exercise, in: 2008 Second Asia International Conference on Modelling & Simulation (AMS), 2008, pp. 963–967. doi:10.1109/AMS.2008.29.
- [25] F. Le, I. Markovskiy, C. T. Freeman, E. Rogers, Identification of electrically stimulated muscle models of stroke patients, *Control engineering practice* 18 (2010) 396–407. doi:10.1016/j.conengprac.2009.12.007.
- [26] Y. Li, M. Zheng, Q. Yang, R. Song, Comparison of two models used to describe the ankle torque in response to functional electrical stimulation, in: 2019 IEEE 4th International Conference on Advanced Robotics and Mechatronics (ICARM), 2019, pp. 894–898. doi:10.1109/ICARM.2019.8834236.
- [27] J.-K. Lim, M.-H. Nam, G. Khang, Model of activation dynamics for an FES-induced muscle fatigue, in: Proceedings of the 22nd Annual International Conference of the IEEE Engineering in Medicine and Bi-

- ology Society (Cat. No.00CH37143), Vol. 3, 2000, pp. 2251–2253 vol.3. doi:10.1109/IEMBS.2000.900587.
- [28] Y. Giat, J. Mizrahi, M. Levy, A musculotendon model of the fatigue profiles of paralyzed quadriceps muscle under FES, *IEEE Transactions on Biomedical Engineering* 40 (7) (1993) 664–674. doi:10.1109/10.237696.
- [29] J. Ding, A. Wexler, S. Binder-Macleod, A predictive fatigue model. i. predicting the effect of stimulation frequency and pattern on fatigue, *IEEE Transactions on Neural Systems and Rehabilitation Engineering* 10 (1) (2002) 48–58. doi:10.1109/TNSRE.2002.1021586.
- [30] R. Riener, T. Fuhr, Patient-driven control of FES-supported standing up: a simulation study, *IEEE Trans Rehabil Eng.* 6 (2) (1998) 113–124. doi:10.1109/86.681177.
- [31] B. Tondu, P. Lopez, Modeling and control of McKibben artificial muscle robot actuators, *IEEE Control Systems Magazine* 20 (2) (2000) 15–38. doi:10.1109/37.833638.
- [32] D. B. Reynolds, D. W. Repperger, C. A. Phillips, G. Bandry, Modeling the dynamic characteristics of pneumatic muscle, *Annals of Biomedical Engineering* 31 (3) (2003) 310–317. doi:10.1114/1.1554921.
- [33] J. E. Slightam, M. L. Nagurka, Robust control law for pneumatic artificial muscles, in: *ASME/BATH 2017 Symposium on Fluid Power and Motion Control*, 2017. doi:10.1115/FPMC2017-4225.
- [34] T. Tagami, T. Miyazaki, T. Kawase, T. Kanno, K. Kawashima, Pressure control of a pneumatic artificial muscle including

- pneumatic circuit model, *IEEE Access* 8 (2020) 60526–60538. doi:10.1109/ACCESS.2020.2983602.
- [35] V. Jouppila, A. Gadsden, A. Ellman, Modeling and identification of a pneumatic muscle actuator system controlled by on/off solenoid valve, in: *Proceedings of the 7th International Fluid Power Conference IFK, Aachen, Germany, 22 - 24 March, 2010*, 2010, pp. 1–34.
- [36] A. Messina, N. I. Giannoccaro, A. Gentile, Experimenting and modelling the dynamics of pneumatic actuators controlled by the pulse width modulation (pwm) technique, *Mechatronics* 15 (7) (2005) 859–881. doi:https://doi.org/10.1016/j.mechatronics.2005.01.003.
- [37] J. Bobrow, B. McDonell, Modeling, identification, and control of a pneumatically actuated, force controllable robot, *IEEE Transactions on Robotics and Automation* 14 (5) (1998) 732–742. doi:10.1109/70.720349.
- [38] Z. Rao, G. M. Bone, Nonlinear modeling and control of servo pneumatic actuators, *IEEE Transactions on Control Systems Technology* 16 (3) (2008) 562–569. doi:10.1109/TCST.2007.912127.
- [39] A. Leardini, J. O’Connor, F. Catani, S. Giannini, A geometric model of the human ankle joint, *Journal of Biomechanics* 32 (6) (1999) 585–591. doi:https://doi.org/10.1016/S0021-9290(99)00022-6.
- [40] C. T. Freeman, A. M. Hughes, J. H. Burridge, P. H. Chappell, P. L. Lewin, E. Rogers, A model of the upper extremity using FES for stroke rehabilitation, *J Biomed Eng.* 131 (3) (2009). doi:10.1115/1.3005332.

- [41] R. Riener, J. Quintern, G. Schmidt, Biomechanical model of the human knee evaluated by neuromuscular stimulation, *Journal of Biomechanics* 29 (9) (1996) 1157–1167. doi:[https://doi.org/10.1016/0021-9290\(96\)00012-7](https://doi.org/10.1016/0021-9290(96)00012-7).
- [42] N. Postans, M. Granat, Effect of functional electrical stimulation, applied during walking, on gait in spastic cerebral palsy, *Developmental medicine and child neurology* 47 (2005) 46–52. doi:[10.1111/j.1469-8749.2005.tb01039.x](https://doi.org/10.1111/j.1469-8749.2005.tb01039.x).
- [43] P. Malcolm, W. Derave, S. Galle, D. Clercq, A simple exoskeleton that assists plantarflexion can reduce the metabolic cost of human walking, *PloS one* 8 (2013) e56137. doi:[10.1371/journal.pone.0056137](https://doi.org/10.1371/journal.pone.0056137).
- [44] H. Lee, E. Rouse, H. Krebs, Summary of human ankle mechanical impedance during walking, *IEEE J Transl Eng Health Med.* 19 (2016) 2100407. doi:[10.1109/JTEHM.2016.2601613](https://doi.org/10.1109/JTEHM.2016.2601613).
- [45] P. L. Weiss, R. E. Kearney, I. W. Hunter, Position dependence of ankle joint dynamics—I. passive mechanics, *Journal of Biomechanics* 19 (9) (1986) 727–735. doi:[10.1016/0021-9290\(86\)90196-x](https://doi.org/10.1016/0021-9290(86)90196-x).
- [46] M. B. Reid, G. J. Grubwieser, D. S. Stokic, S. M. Koch, A. A. Leis, Development and reversal of fatigue in human tibialis anterior, *Muscle & Nerve* 16 (11) (1993) 1239–45.
- [47] S. J. Kim, J. Park, W. Shin, D. Y. Lee, J. Kim, Proof-of-concept of a pneumatic ankle foot orthosis powered by a custom compressor for drop foot correction, in: 2020 IEEE International Con-

- ference on Robotics and Automation (ICRA), 2020, pp. 747–753. doi:10.1109/ICRA40945.2020.9196817.
- [48] N. Kurokawa, N. Yamamoto, Y. Tagawa, T. Yamamoto, H. Kuno, Development of hybrid fes walking assistive system - feasibility study-, in: The 2012 International Conference on Advanced Mechatronic Systems, 2012, pp. 93–97.
- [49] Y.-L. Park, B.-r. Chen, N. O. PÃ©rez-Arancibia, D. Young, L. Stirling, R. J. Wood, E. C. Goldfield, R. Nagpal, Design and control of a bio-inspired soft wearable robotic device for ankle foot rehabilitation, *Bioinspiration & Biomimetics* 9 (2014) 016007. doi:10.1088/1748-3182/9/1/016007.
- [50] D. Ferris, J. Czerniecki, B. Hannaford, An ankle-foot orthosis powered by artificial pneumatic muscles, *Journal of Applied Biomechanics* 21 (2005) 189–97. doi:10.1123/jab.21.2.189.
- [51] M. Khoobani, M. Nazari, N. Sepehry, M. Ameri, N. Sahebi, A personalized fes-assisted foot drop correction device via a real-time fuzzy controller based on the patient’s healthy foot condition, in: 2021 9th RSI International Conference on Robotics and Mechatronics (ICRoM), 2021, pp. 497–503. doi:10.1109/ICRoM54204.2021.9663462.
- [52] E. H. Copur, C. T. Freeman, B. Chu, D. S. Laila, System identification for FES-based tremor suppression, *European Journal of Control* 27 (2016) 45–59. doi:https://doi.org/10.1016/j.ejcon.2015.12.003.

- [53] K. Yang, K. Meadmore, C. Freeman, N. Grabham, A.-M. Hughes, Y. Wei, R. Torah, M. Glanc-Gostkiewicz, S. Beeby, M. Tudor, Development of user-friendly wearable electronic textiles for healthcare applications, *Sensors* 18 (8) (2018) 1–13.